Origami/Kirigami-Inspired Reconfigurable 6*R* Linkages and Tessellations

Weiqi Liu and Yan Chen

Abstract Reconfigurable structures are considered promising candidates for high-adaptability and multi-functionality due to their variable topology and have thus gained thriving progress in recent years. To date, most studies on reconfigurable linkages focus on innovative design and reconfiguration mechanism of a single unit, yet the possibility of forming larger structures is rarely investigated. In this paper, we develop a multi-loop origami pattern with flat foldability and rigid foldability formed by four 4-crease vertices, which can be utilized as a platform for constructing reconfigurable 6*R* linkages. Through the analysis of kinematic compatibility of equivalent networks of spherical linkages, three types of reconfigurable 6*R* linkages are obtained with the kirigami technique, including a double spherical linkage, a planar-spherical linkage, and a parallel 6*R* linkage. The explicit closure equations and bifurcation behaviors of obtained parallel 6*R* linkage have been derived. Connecting the linkage under bifurcation paths, the tessellation of this parallel 6*R* linkage forms a series of structures with complex shapes with one DOF, e.g., arch shapes, "m" shape, and closed-loop tube, whose reconfigurability is achieved simply by switching some mountain and valley creases. This work provides a promising perspective for constructing reconfigurable 6*R* linkages from origami and kirigami, which can be applied in deployable structures, architectures, homogeneous or heterogeneous metamaterials.

Keywords origami/kirigami · 6*R* linkage · Rigid foldability · Reconfigurability · Parallel 6*R* linkage

W. Liu · Y. Chen (✉)
Key Laboratory of Mechanism Theory and Equipment Design of Ministry of Education, Tianjin, China
e-mail: yan_chen@tju.edu.cn

School of Mechanical Engineering, Tianjin University, Tianjin 300350, China

© The Author(s), under exclusive license to Springer Nature Singapore Pte Ltd. 2023

X. Liu (ed.), *Advances in Mechanism, Machine Science and Engineering in China*,
Lecture Notes in Mechanical Engineering,
https://doi.org/10.1007/978-981-19-9398-5_82

1 Introduction

Origami and kirigami [1, 2] both originated from the paper art of transforming 2D sheet materials into 3D structures along designed crease patterns, and origami focuses on folding without cutting while kirigami involves cutting. This striking morphing ability enables origami/kirigami-inspired structures in recent years to attract substantial attention for application scenarios in robotics [3], aerospace engineering [4], bioengineering [5], and so on. Due to the diversity and scale-free nature of the geometry, origami/kirigami with excellent design flexibility has also provided valuable guidelines for designing metamaterials with unique mechanical properties. Among them, kinematic metamaterials [6] derived from rigid origami/kirigami are particularly appreciated due to stable and predictable deformation paths. Up to now, rigid patterns with single-degree-of-freedom (DOF), such as Miura-ori and its variations [7], square-twist [8], generalized quadrilateral-mesh [9], double corrugated [10], and so on, have been extensively studied. A notable feature of these patterns is that they are the tessellations of four 4-crease vertices with identical topology, i.e., quadrilateral-mesh, which consists of a central quadrilateral plus two extended creases from each vertex. It is an urgent need to develop new origami patterns with unique topologies for prospering applications. On the other hand, current studies focus on origami patterns that morph between final configurations along a single mountain-valley (M-V) assignment. Recently, it was revealed that different M-V assignments correspond to different bifurcation paths of the crease pattern after passing through the singular point [10]. This bifurcation behavior may cause essential changes in properties, making reconfigurable origami/kirigami-inspired structures more suitable for multifunctional applications. For instance, morph pattern [11, 12] displays switchable Poisson's Ratio (a tuneability between positive and negative) as it undergoes topological morphing between an Eggbox mode and a Miura mode by breaking M-V assignments.

The innovative design of such reconfigurable origami/kirigami-inspired structures is essentially the design for reconfigurable linkages, as the creases and panels in the crease pattern can be modeled as revolute (R) joints and links of the linkage [13], respectively. For instance, the best-known one-DOF rigid vertex with four creases intersecting at one point which is kinematically a spherical 4R linkage. Hence, a rigid origami pattern with multiple vertices e.g., quadrilateral-mesh, can be regarded as a mobile network of spherical linkages [14–16]. Such interdisciplinary studies on rigid origami/kirigami and linkage not only provide a way to investigate the motion behavior of creases patterns, but also shed a bright light on designing reconfigurable linkages. A variety of mechanisms [17–23] with reconfigurability was developed through the mapping from origami/kirigami to kinematic structures. Yet, the possibility of these reconfigurable units forming larger structures has rarely been discussed, which limits the further application of these units in deployable structures, architectures, and metamaterials, where the tessellation is a mandatory requirement.

In this paper, we develop a multi-loop origami pattern with flat foldability and rigid foldability formed by four 4-crease vertices. It can be utilized as a platform for

constructing reconfigurable 6*R* linkages by applying the kirigami technique. Furthermore, we demonstrate the unique advantage of obtained reconfigurable linkages in building larger homogeneous or heterogeneous structures with complex shapes through tessellating their corresponding crease patterns. Finally, the discussion and conclusions end this paper.

2 Crease Patterns and Corresponding Linkage Forms

2.1 Origami Pattern and Its Rigid Foldability and Reconfigurability

The quadrilateral-mesh is the basis for most well-studied rigid origami patterns [7–10], in which four vertices form a rigid quadrilateral in the center, and two extended creases from each vertex. Obviously, the kirigami pattern formed by removing the center quadrilateral of the single DOF origami pattern is a 2-DOF 8*R* linkage. In this study, we developed a double-triangle mesh origami also formed by four 4-crease vertices as shown in Fig. 1a, where a_i, b_i, c_i, d_i $(i = 1, 2, 3, 4)$ are axes of creases, and $\alpha^a_{i(i+1)}, \alpha^b_{i(i+1)}, \alpha^c_{i(i+1)}, \alpha^d_{i(i+1)}$ are sector angles on vertices A, B, C, D, respectively. It differs from the former in that vertices A and D share a pair of creases b_2, d_1. Thus, four vertices form two rigid triangles ABD, BCD, and a total of six extended creases on these four vertices. Each vertex can be modeled as a spherical 4*R* linkage. Hence, the origami pattern shown in Fig. 1a is kinematically equivalent to a multi-loop network of spherical 4*R* linkages. Figure 1b shows its topology graph in which each line represents a crease or joint and a black solid dot represents a panel or link. We can tell the pattern shown in Fig. 1a and the quadrilateral-mesh pattern are of different topology according to their topological graphs.

A closed-loop pattern is said to be rigidly foldable only if the motion transmitted through the creases finally returns to input, which is also the compatibility condition of the corresponding linkage form. For the multi-loop network of spherical 4*R* linkage in Fig. 2, the rotation angles of shared joints are equal, so $\theta^a_2 = \theta^b_1$, $\theta^b_2 = \theta^d_1$, $\theta^d_2 = \theta^a_1$, $\theta^b_3 = \theta^c_1$ and $\theta^c_2 = \theta^d_4$. The transmission paths of kinematic motion for the closed loops ABD, BCD, and ABCD in Fig. 2 are

$$\theta^a_1 \longrightarrow \theta^a_2 = \theta^b_1 \longrightarrow \theta^b_2 = \theta^d_1 \longrightarrow \theta^d_2, \quad \theta^a_1 = \theta^d_2 \tag{1a}$$

$$\theta^b_2 \longrightarrow \theta^b_3 = \theta^c_1 \longrightarrow \theta^c_2 = \theta^d_4 \longrightarrow \theta^d_1, \quad \theta^b_2 = \theta^d_1 \tag{1b}$$

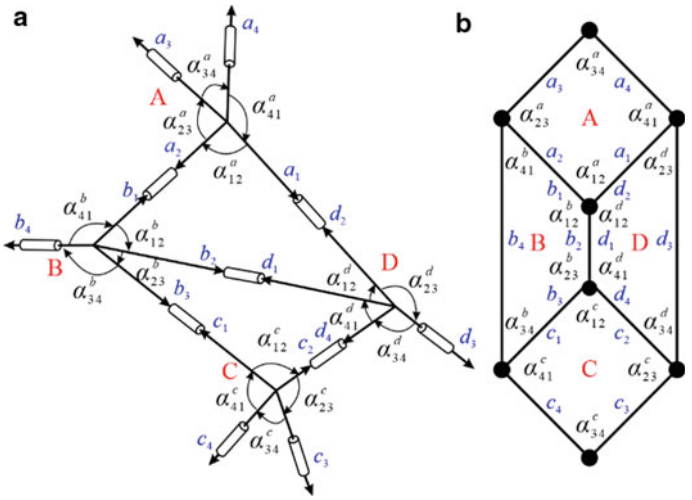

Fig. 1 Transition from origami pattern to linkage form with topological graph

$$\theta_1^a \longrightarrow \theta_2^a=\theta_1^b \longrightarrow \theta_3^b=\theta_1^c \longrightarrow \theta_2^c=\theta_4^d \longrightarrow \theta_2^d \quad \theta_1^a=\theta_2^d, \tag{1c}$$

respectively, which can be written as

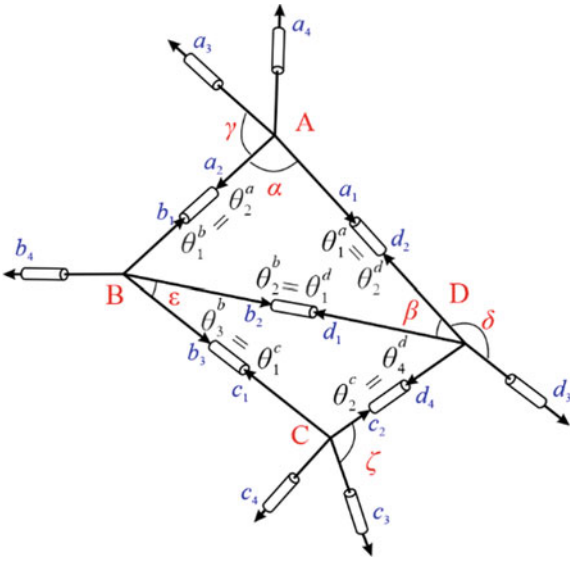

Fig. 2 Relationships between rotation angles in double-triangle mesh origami

$$\frac{\tan\frac{\theta_1^a}{2}}{\tan\frac{\theta_2^d}{2}} = \frac{\tan\frac{\theta_1^a}{2}}{\tan\frac{\theta_2^a}{2}} \cdot \frac{\tan\frac{\theta_1^b}{2}}{\tan\frac{\theta_2^b}{2}} \cdot \frac{\tan\frac{\theta_1^d}{2}}{\tan\frac{\theta_2^d}{2}}, \tag{2a}$$

$$\frac{\tan\frac{\theta_2^b}{2}}{\tan\frac{\theta_1^d}{2}} = \frac{\tan\frac{\theta_2^b}{2}}{\tan\frac{\theta_3^b}{2}} \cdot \frac{\tan\frac{\theta_1^c}{2}}{\tan\frac{\theta_2^c}{2}} \cdot \frac{\tan\frac{\theta_4^d}{2}}{\tan\frac{\theta_1^d}{2}}, \tag{2b}$$

$$\frac{\tan\frac{\theta_1^a}{2}}{\tan\frac{\theta_2^d}{2}} = \frac{\tan\frac{\theta_1^a}{2}}{\tan\frac{\theta_2^a}{2}} \cdot \frac{\tan\frac{\theta_1^b}{2}}{\tan\frac{\theta_3^b}{2}} \cdot \frac{\tan\frac{\theta_1^c}{2}}{\tan\frac{\theta_2^c}{2}} \cdot \frac{\tan\frac{\theta_4^d}{2}}{\tan\frac{\theta_2^d}{2}}. \tag{2c}$$

It is noted that when two of Eqs. (2a)–(2c) hold, the third one is automatically satisfied.

Due to the flat foldability condition [1], i.e., the sum of the alternative sector angles about one vertex is equal to π, the crease pattern in Fig. 2 can be fully defined by six geometric parameters α, β, γ, ε, δ, ζ. The relationships between rotation angles θ_i of a 4-crease vertex [21] following the D-H method [24] (in Appendix 1) are

$$\theta_1 = -\theta_3, \quad \theta_2 = \theta_4, \quad \frac{\tan\frac{\theta_1}{2}}{\tan\frac{\theta_2}{2}} = -\frac{\sin\frac{\alpha_{23}-\alpha_{12}}{2}}{\sin\frac{\alpha_{23}+\alpha_{12}}{2}}, \tag{3a}$$

and

$$\theta_1 = \theta_3, \quad \theta_2 = -\theta_4, \quad \frac{\tan\frac{\theta_1}{2}}{\tan\frac{\theta_2}{2}} = -\frac{\cos\frac{\alpha_{23}-\alpha_{12}}{2}}{\cos\frac{\alpha_{23}+\alpha_{12}}{2}}, \tag{3b}$$

for two distinct M-V assignments, i.e., Vertex-I and Vertex-II in Fig. 3, respectively.

Considering whether vertices A, B, C, D belong to Vertex-I or Vertex-II, there are a total of 8 cases for the closed loops ABD, i.e., $A_IB_ID_I$, $A_IB_ID_{II}$, $A_IB_{II}D_I$, $A_IB_{II}D_{II}$, $A_{II}B_ID_I$, $A_{II}B_ID_{II}$, $A_{II}B_{II}D_I$, $A_{II}B_{II}D_{II}$, where the subscript represents the type of the vertex. Thus, Eq. (2a) can be sorted out as

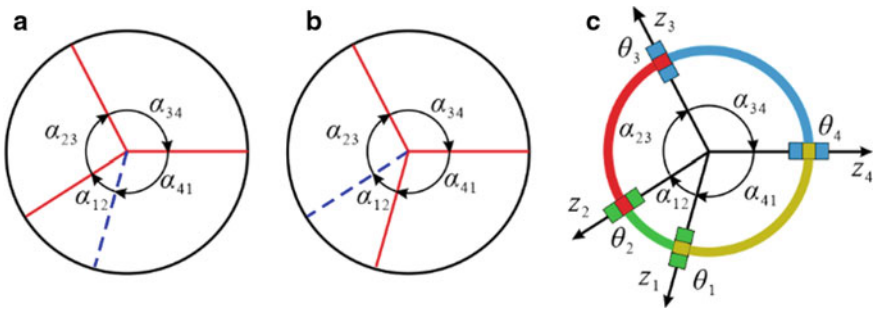

Fig. 3 A 4-crease vertex and its linkage form: **a** vertex-I, **b** vertex-II, and **c** its linkage form

$$f(\mathrm{A_I B_I D_I}) = \frac{-\cos E_1 + \cos E_2 + \cos E_3 - \cos E_0}{-\cos E_4 + \cos E_5 + \cos E_6 - \cos E_0} = 1, \tag{4a}$$

$$f(\mathrm{A_I B_I D_{II}}) = \frac{\sin E_1 + \sin E_2 - \sin E_3 - \sin E_0}{-\sin E_4 - \sin E_5 + \sin E_6 - \sin E_0} = 1, \tag{4b}$$

$$f(\mathrm{A_I B_{II} D_I}) = \frac{\sin E_1 - \sin E_2 - \sin E_3 + \sin E_0}{-\sin E_4 + \sin E_5 + \sin E_6 + \sin E_0} = 1, \tag{4c}$$

$$f(\mathrm{A_I B_{II} D_{II}}) = \frac{-\cos E_1 - \cos E_2 + \cos E_3 + \cos E_0}{-\cos E_4 - \cos E_5 + \cos E_6 + \cos E_0} = 1, \tag{4d}$$

$$f(\mathrm{A_{II} B_I D_I}) = \frac{-\sin E_1 + \sin E_2 - \sin E_3 + \sin E_0}{\sin E_4 - \sin E_5 + \sin E_6 + \sin E_0} = 1, \tag{4e}$$

$$f(\mathrm{A_{II} B_I D_{II}}) = \frac{-\sin E_1 + \sin E_2 - \sin E_3 + \sin E_0}{\sin E_4 - \sin E_5 + \sin E_6 + \sin E_0} = 1, \tag{4f}$$

$$f(\mathrm{A_{II} B_{II} D_I}) = \frac{\cos E_1 - \cos E_2 + \cos E_3 - \cos E_0}{\cos E_4 - \cos E_5 + \cos E_6 - \cos E_0} = 1, \tag{4g}$$

$$f(\mathrm{A_{II} B_{II} D_{II}}) = \frac{-\sin E_1 - \sin E_2 - \sin E_3 - \sin E_0}{\sin E_4 + \sin E_5 + \sin E_6 - \sin E_0} = 1, \tag{4h}$$

where

$$E_0 = (\gamma + \delta + \varepsilon)/2,\ E_1 = \alpha + \beta - (\gamma + \delta - \varepsilon)/2,$$

$$E_2 = \alpha - (\gamma - \delta - \varepsilon)/2,\ E_3 = \beta + (\gamma - \delta + \varepsilon)/2,$$

$$E_4 = \alpha + \beta + (\gamma + \delta - \varepsilon)/2,\ E_5 = \alpha + (\gamma - \delta - \varepsilon)/2,$$

$$E_6 = \beta - (\gamma - \delta + \varepsilon)/2.$$

Meanwhile, 16 cases for the closed loops ABCD, i.e., $\mathrm{A_I B_I C_I D_I}$, $\mathrm{A_I B_I C_{II} D_I}$, $\mathrm{A_I B_I C_I D_{II}}$, $\mathrm{A_I B_I C_{II} D_{II}}$, $\mathrm{A_I B_{II} C_I D_I}$, $\mathrm{A_I B_{II} C_{II} D_I}$, $\mathrm{A_I B_{II} C_I D_{II}}$, $\mathrm{A_I B_{II} C_{II} D_{II}}$, $\mathrm{A_{II} B_I C_I D_I}$, $\mathrm{A_{II} B_I C_{II} D_I}$, $\mathrm{A_{II} B_I C_I D_{II}}$, $\mathrm{A_{II} B_I C_{II} D_{II}}$, $\mathrm{A_{II} B_{II} C_I D_I}$, $\mathrm{A_{II} B_{II} C_{II} D_I}$, $\mathrm{A_{II} B_{II} C_I D_{II}}$, $\mathrm{A_{II} B_{II} C_{II} D_{II}}$. Thus, Eq. (2c) can be sorted out as

$$f(\mathrm{A_I B_I C_I D_I}) = f(\mathrm{A_I B_{II} C_I D_{II}}) = \frac{\cos F_1 - \cos F_2}{\cos F_3 - \cos F_4} = 1, \tag{5a}$$

$$f(\mathrm{A_I B_I C_{II} D_I}) = f(\mathrm{A_I B_{II} C_{II} D_{II}}) = \frac{\sin F_1 + \sin F_2}{\sin F_3 + \sin F_4} = 1, \tag{5b}$$

$$f(\mathrm{A_I B_I C_I D_{II}}) = f(\mathrm{A_I B_{II} C_I D_I}) = \frac{-\cos F_1 + \cos F_2}{\cos F_3 - \cos F_4} = 1, \tag{5c}$$

$$f(\mathrm{A_I B_I C_{II} D_{II}}) = f(\mathrm{A_I B_{II} C_{II} D_I}) = \frac{-\sin F_1 - \sin F_2}{\sin F_3 + \sin F_4} = 1, \tag{5d}$$

$$f(\mathrm{A_{II} B_I C_I D_I}) = f(\mathrm{A_{II} B_{II} C_I D_{II}}) = \frac{-\sin F_1 + \sin F_2}{\sin F_3 - \sin F_4} = 1, \tag{5e}$$

$$f(\mathrm{A_{II} B_I C_{II} D_I}) = f(\mathrm{A_{II} B_{II} C_{II} D_{II}}) = \frac{-\cos F_1 - \cos F_2}{\cos F_3 + \cos F_4} = 1, \tag{5f}$$

$$f(\mathrm{A_{II} B_I C_I D_{II}}) = f(\mathrm{A_{II} B_{II} C_I D_I}) = -\frac{-\sin F_1 + \sin F_2}{\sin F_3 - \sin F_4} = 1, \tag{5g}$$

$$f(\mathrm{A_{II} B_I C_{II} D_{II}}) = f(\mathrm{A_{II} B_{II} C_{II} D_I}) = \frac{\cos F_1 + \cos F_2}{\cos F_3 + \cos F_4} = 1, \tag{5h}$$

where $F_1 = (\alpha + \delta - \varepsilon - \gamma - \zeta)/2$, $F_2 = (\alpha - \delta + \varepsilon - \gamma + \zeta)/2$, $F_3 = (\alpha - \delta + \varepsilon + \gamma - \zeta)/2$, $F_4 = (\alpha + \delta - \varepsilon + \gamma + \zeta)/2$.

Equations (4a)–(4h) and (5a)–(5h) are necessary and sufficient conditions for the rigid foldability of double-triangle mesh origami. Each equation includes two parts of information: geometric parameters and vertex type, i.e., the geometry of an arbitrary rigid pattern must satisfy one of Eqs. (4a)–(4h) and one of (5a)–(5h), and A, B and D in these two equations are vertices of the same type. This makes it possible to evaluate the rigid foldability of the origami pattern and then derive M-V arrangements when only the geometric parameters are given. Special geometric parameters may lead to several sets of equations in (4a)–(4h) and (5a)–(5h) being satisfied simultaneously, leading to different M-V arrangements. Namely, Eqs. (4a)–(4h) and (5a)–(5h) can also be utilized to evaluate the reconfigurability of origami patterns. Apparently, many angle parameters could satisfy these non-linear equations. In addition to the numerical method, we can derive some special solutions with assumptions such as parallel or symmetry conditions as premises.

2.2 *Case Studies on Evaluation of Rigid-Foldability and Reconfigurability of Origami Patterns*

Here we treat double-triangle mesh origami as a combination of two triangle twists. As shown in Fig. 4, triangle twist consists of a central triangle plus two extended creases from each vertex of the triangle. In order to merge two triangle twist patterns P and Q together, they have to share two common vertices and creases in these vertices. There are only two types of rigid foldable triangle twists under a specific M-V assignment [21], i.e., twist $\mathrm{T_1}$ with no parallel crease-pair and twist $\mathrm{T_2}$ with one parallel crease-pair. Hence, there are four possible combinations with $\mathrm{T_1}$ and

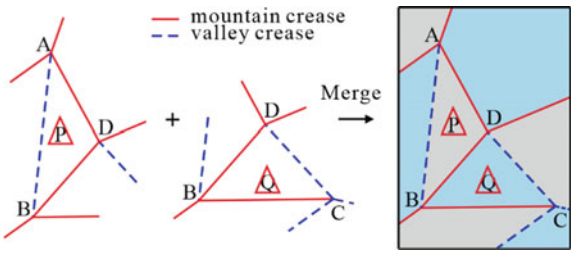

Fig. 4 A diagram of the merging of two triangle twists into a kirigami pattern, where M-V creases are represented by the red solid lines and blue dotted lines

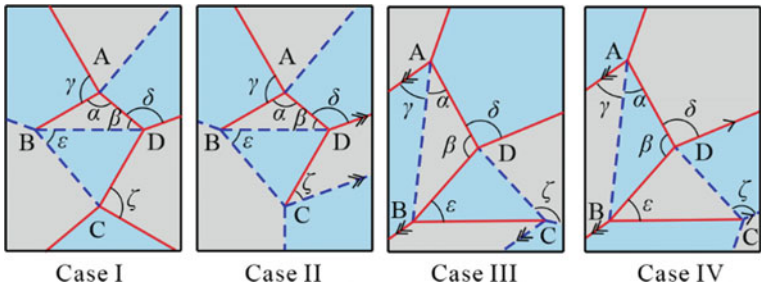

Fig. 5 Four possible combinations of origami patterns with geometry parameters, where case I is $T_1 + T_1$, case II is $T_1 + T_2$, and $T_2 + T_2$ in cases III and IV

T_2 as shown in Fig. 5, where the arrow on the crease is for a parallel symbol. Case I is the combination of two T_1, while case II is for $T_1 + T_2$. Considering whether the parallel crease-pairs are adjacent or not, there are two cases, III and IV, for the combinations of two T_2.

The rigid foldability and reconfigurability of four merged origami patterns will be explored one by one. As illustrated in Fig. 5, case I is formed by two twists T_1 with no parallel creases. The parameters and M-V assignments of case I are the same as asymmetric level shifter in Ref. [25]. Its geometry parameters are

$$\begin{aligned} &\alpha = \pi - \alpha_0 - \beta_0, \quad \beta = \beta_0, \quad \gamma = \pi/2, \\ &\varepsilon = \pi/2 - \beta_0, \quad \delta = \pi/2 + \alpha_0, \quad \zeta = \pi/2 \end{aligned} \tag{6}$$

When $\alpha_0 + \beta_0 = \pi/2$, it is an excluded case where the sector angles of vertices A and C are all right angles. The sum of the two opposite angles should be π, so $\alpha_0, \beta_0 < \pi/2$. Substituting the given parameters into Eqs. (4a)–(4h) and (5a)–(5h), we can obtain two sets of solutions, $f(A_I B_{II} D_{II}) = 1$, $f(A_I B_{II} C_{II} D_{II}) = 1$ and $f(A_{II} B_I D_I) = 1$, $f(A_{II} B_I C_I D_I) = 1$, that satisfy the compatibility conditions of its linkage form in Fig. 6a. Thus, the origami pattern of case I is rigidly foldable with $\alpha_0, \beta_0 < \pi/2$ and $\alpha_0 + \beta_0 \neq \pi/2$. Moreover, the origami pattern of case I exists two

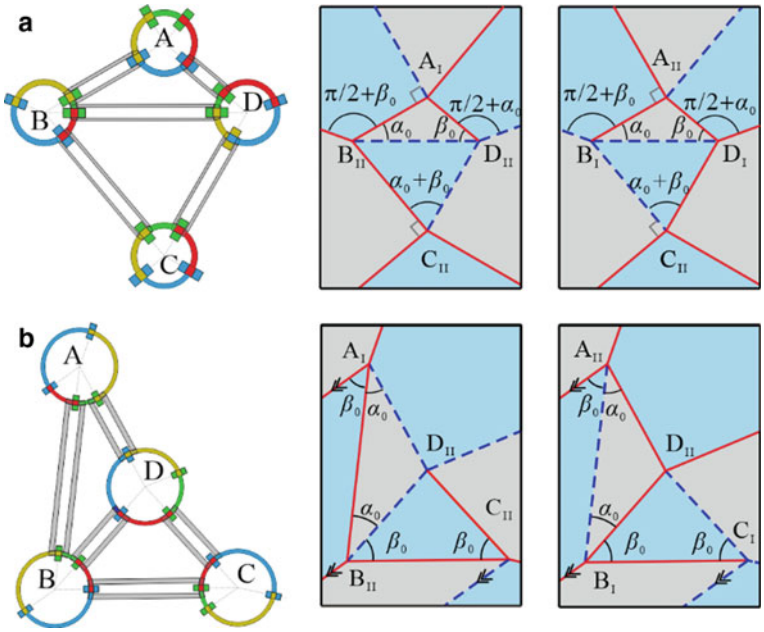

Fig. 6 Linkage form and M-V assignments of origami cases I and III. The subscript of A, B, C, D represents the type of the vertex

different M-V assignments that correspond to these two sets of solutions respectively, as shown in Fig. 6a.

The origami pattern of case II in Fig. 5 consists of two different types of twists T_I and T_2, and its geometry conditions are

$$\begin{aligned} &\alpha = \pi - \alpha_0 - \beta_0, \quad \beta = \beta_0, \quad \gamma = \pi/2, \\ &\varepsilon = \pi/2 - \beta_0, \quad \delta = \pi/2 + \alpha_0, \quad \zeta = \beta_0. \end{aligned} \tag{7}$$

It proved to be incompatible as Eqs. (5a)–(5h) are not satisfied under the geometry parameters listed in Eq. (7). So, the origami pattern of case II is non-rigidly foldable.

The origami pattern of case III is obtained by merging two twists T_2, where two sets of parallel creases are placed on the adjacent creases. As shown in Fig. 5, the parameters and M-V assignments are the same as the triple parallel gadget in Ref. [25]. The geometry conditions are

$$\begin{aligned} &\alpha = \alpha_0, \quad \beta = \pi - 2\alpha_0, \quad \gamma = \beta_0, \\ &\varepsilon = \beta_0, \quad \delta = 2\beta_0, \quad \zeta = \pi - \alpha_0. \end{aligned} \tag{8}$$

When $\alpha_0 = \beta_0$, the axes of the joints b_2, b_4, d_1, d_3 are collinear, and this case is excluded. The sum of the internal angles of triangle ABD, BCD is equal to π,

thus α_0, $\beta_0 < \pi/2$. For the origami pattern of case III, we obtain $f(\mathrm{A_I B_{II} D_{II}}) = 1$, $f(\mathrm{A_I B_{II} C_{II} D_{II}}) = 1$ and $f(\mathrm{A_{II} B_I D_{II}}) = 1$, $f(\mathrm{A_{II} B_I C_I D_{II}}) = 1$ that satisfy compatibility conditions of its linkage form in Fig. 6b. Therefore, this pattern is rigidly foldable for α_0, $\beta_0 < \pi/2$ and $\alpha_0 \neq \beta_0$. Similarly, two different M-V assignments correspond to these two sets of solutions respectively, as shown in Fig. 6b.

Similar to case II, the pattern of case IV does not satisfy the compatibility conditions of Eqs. (5a)–(5h) under the geometry conditions listed in Eq. (9), and it is also proved to be non-rigidly foldable.

$$\begin{aligned} &\alpha = \alpha_0, \quad \beta = \pi - 2\alpha_0, \quad \gamma = \beta_0, \\ &\varepsilon = \beta_0, \quad \delta = 2\beta_0, \quad \zeta = \pi - 2\alpha_0. \end{aligned} \tag{9}$$

2.3 *Kirigami Pattern and Corresponding 6*R *Linkage*

Inspired by the construct approaches of Goldberg linkages [26], i.e., summation or subtraction approach, kirigami techniques can also be used for the double-triangle mesh origami. Removing two triangle panels in the center obtains the kirigami pattern with six creases in Fig. 7, which also can be regarded as a 6*R* linkage.

Two of the four origami patterns have been proved to be rigidly foldable with compatibility conditions, i.e., case I and case III. After removing △ABD and △BCD, the kirigami patterns and their equivalent linkage forms are shown in Fig. 8a and b, respectively. It can be found that the 6*R* linkage in Fig. 8a is in fact a double spherical

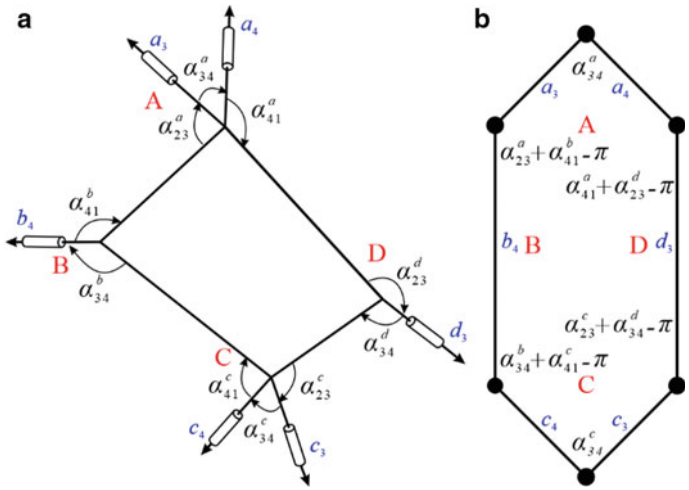

Fig. 7 Single-loop kirigami pattern with six creases and its topological graph

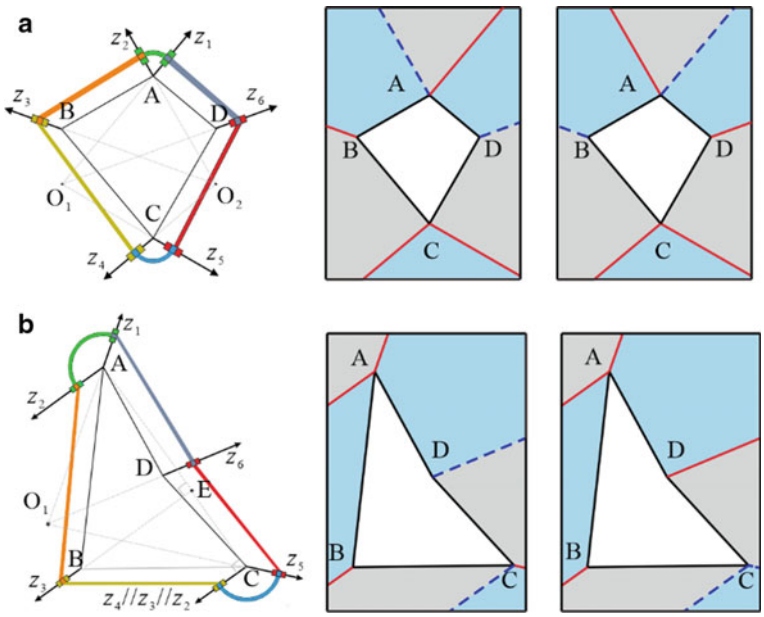

Fig. 8 Linkage form and M-V assignments of kirigami cases I and III

linkage with two sets of three concurrent *R*-joints, the one in Fig. 8b is a planar-spherical linkage with three joints intersecting one point and another three joints parallel. As shown in Fig. 8a and b, both 6*R* linkages inherit the reconfigurability (different M-V assignments) derived from origami patterns. The reconfigurable 6*R* linkage can be constructed by first finding the geometric parameters that satisfy multiple sets of solutions, and then applying the kirigami technique to the double-triangle mesh origami.

Another interesting and critical question is what will happen if we remove two central triangles from non-rigidly foldable origami patterns of cases II and IV. As derived in Appendix 2, the kirigami pattern of case II is non-rigidly foldable. Meanwhile, kirigami pattern of case IV, also named *parallel 6-crease* kirigami pattern, exists three pairs of parallel creases as shown in Fig. 9. To investigate its rigid foldability, we model the crease and the panel as joints and links respectively. Its geometric conditions following D-H notations are

$$\begin{aligned} &a_{12} = 0, \quad a_{23} = a, \quad a_{34} = 0, \\ &a_{45} = 0, \quad a_{56} = \frac{a \sin \alpha_0}{\sin \beta_0}, \quad a_{61} = 0, \end{aligned} \tag{10a}$$

$$\begin{aligned} &\alpha_{12} = \pi - \alpha_0, \quad \alpha_{23} = 0, \quad \alpha_{34} = \alpha_0, \\ &\alpha_{45} = \pi - \beta_0, \quad \alpha_{56} = 0, \quad \alpha_{61} = \beta_0, \end{aligned} \tag{10b}$$

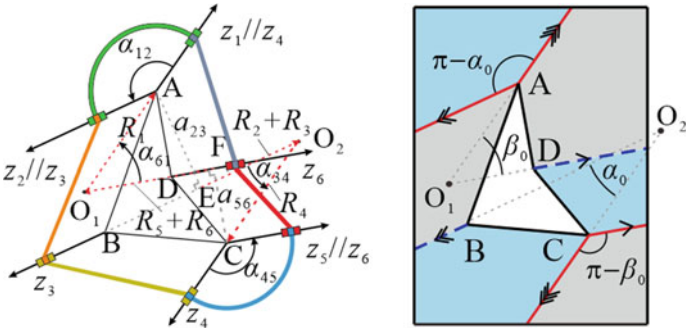

Fig. 9 *Parallel 6-crease* kirigami pattern and its linkage form

$$\begin{aligned} R_1 &= \overline{O_1A} = \frac{a}{\tan\beta_0\cos\alpha_0}, \quad R_2 + R_3 = -\overline{EO_2} = -\frac{a}{\tan\beta_0}, \\ R_4 &= \overline{O_2C} = \frac{a}{\tan\beta_0\cos\alpha_0}, \quad R_5 + R_6 = -\overline{FO_1} = -\frac{a\cos\alpha_0}{\sin\beta_0}. \end{aligned} \tag{10c}$$

3 Kinematic Properties of Parallel 6*R* Linkage

For this *parallel 6-crease* kirigami pattern, the loop closure equation of its linkage form can be derived as

$$\boldsymbol{T}_{65}\boldsymbol{T}_{54}\boldsymbol{T}_{43} - \boldsymbol{T}_{61}\boldsymbol{T}_{12}\boldsymbol{T}_{23} = 0. \tag{11}$$

Substituting geometric parameters in Eqs. (10a)–(10c) into Eq. (11), the simplified element (3, 3) of 16 equations in Eq. (11) is

$$\sin\alpha_0\sin\beta_0(\cos\theta_1 - \cos\theta_4) = 0. \tag{12}$$

We can get

$$\theta_1 = \pm\theta_4. \tag{13}$$

When $\theta_1 = \theta_4$, elements (3, 1) and (3, 2) can be simplified as

$$\begin{aligned} &(\cos\beta_0\sin\alpha_0 - \cos\alpha_0\sin\beta_0\cos\theta_1)(\sin\theta_2 + \sin\theta_3) \\ &\quad + \sin\beta_0\sin\theta_1(\cos\theta_2 - \cos\theta_3) = 0, \end{aligned} \tag{14}$$

and

$$(\cos\beta_0 \sin\alpha_0 - \cos\alpha_0 \sin\beta_0 \cos\theta_1)(\cos\theta_2 - \cos\theta_3) - \sin\beta_0 \sin\theta_1(\sin\theta_2 + \sin\theta_3) = 0. \tag{15}$$

There are two sets of solutions for Eqs. (14) and (15), one is

$$\cos\beta_0 \sin\alpha_0 - \cos\alpha_0 \sin\beta_0 \cos\theta_1 = 0, \tag{16}$$

and

$$\sin\beta_0 \sin\theta_1 = 0. \tag{17}$$

Equations (16) and (17) yield

$$\theta_1 = 0, \quad \alpha_0 = \beta_0. \tag{18}$$

This case is excluded because the axes of the joints z_3, z_6 are collinear. The other one is

$$\sin\theta_2 + \sin\theta_3 = 0, \tag{19}$$

and

$$\cos\theta_2 - \cos\theta_3 = 0. \tag{20}$$

Equations (19) and (20) yield

$$\theta_2 + \theta_3 = 0. \tag{21}$$

The loop closure equation can also be rewritten as

$$T_{21}T_{32}T_{43} - T_{61}T_{56}T_{45} = 0. \tag{22}$$

The simplified element (3, 3) of 16 equations in Eq. (22) are

$$\cos^2\beta_0 + \sin^2\beta_0 \cos(\theta_5 + \theta_6) = \cos^2\alpha_0 + \sin^2\alpha_0 \cos(\theta_2 + \theta_3). \tag{23}$$

We can get the relationship between θ_5 and θ_6 as follow

$$\theta_5 + \theta_6 = 0. \tag{24}$$

Element (3, 4) can be simplified as

$$\cos^3\beta_0 \cos(\theta_5 + \theta_6) - \cos^3\beta_0 - \cos\beta_0 \cos(\theta_5 + \theta_6) + \cos\beta_0 + \cos\alpha_0 \sin\alpha_0 \sin\beta_0(\sin\theta_2 + \sin\theta_6) = 0. \tag{25}$$

Then, substituting Eq. (24) into Eq. (25), we will get

$$\theta_2 + \theta_6 = 0, \tag{26}$$

and

$$\theta_2 - \theta_6 = \pi. \tag{27}$$

Moreover, the other kinematic variables θ_1 and θ_2 can be calculated by substituting Eq. (24) to the element (1, 4), i.e.,

$$\begin{aligned}&\sin\alpha_0\cos\theta_6 - \cos\beta_0\sin\alpha_0\sin\theta_1 + \sin\beta_0\cos\theta_1\cos\theta_2\\&\quad + \cos\alpha_0\sin\beta_0\sin\theta_1\sin\theta_2 = 0.\end{aligned} \tag{28}$$

When $\theta_2 + \theta_6 = 0$, Eq. (28) can be simplified as

$$\tan\frac{\theta_1}{2} = \frac{\cos\left(\frac{\alpha_0-\beta_0}{2}\right)\left(\cos\frac{\theta_2}{2} + \sin\frac{\theta_2}{2}\right)}{\cos\left(\frac{\alpha_0+\beta_0}{2}\right)\left(\cos\frac{\theta_2}{2} - \sin\frac{\theta_2}{2}\right)}. \tag{29}$$

And when $\theta_2 - \theta_6 = \pi$, Eq. (28) can be further simplified as

$$\tan\frac{\theta_1}{2} = -\frac{\sin\left(\frac{\alpha_0-\beta_0}{2}\right)\left(\cos\frac{\theta_2}{2} + \sin\frac{\theta_2}{2}\right)}{\sin\left(\frac{\alpha_0+\beta_0}{2}\right)\left(\cos\frac{\theta_2}{2} - \sin\frac{\theta_2}{2}\right)}. \tag{30}$$

Next, let's consider the case of $\theta_1 = -\theta_4$, elements (3, 1) and (3, 2) of 16 equations in Eq. (22) are

$$\begin{aligned}&(\cos\beta_0\sin\alpha_0 - \cos\alpha_0\sin\beta_0\cos\theta_1)(\sin\theta_2 + \sin\theta_3)\\&\quad + \sin\beta_0\sin\theta_1(\cos\theta_2 + \cos\theta_3) = 0,\end{aligned} \tag{31}$$

and

$$\begin{aligned}&(\cos\beta_0\sin\alpha_0 - \cos\alpha_0\sin\beta_0\cos\theta_1)(\cos\theta_2 - \cos\theta_3)\\&\quad + \sin\beta_0\sin\theta_1(\sin\theta_3 - \sin\theta_2) = 0.\end{aligned} \tag{32}$$

There are also two set of possible solutions for Eqs. (31) and (32). One is $\theta_1 = 0$, $\alpha_0 = \beta_0$, which is consistent with case in Eq. (18). The second set of solutions is

$$\sin\theta_2 + \sin\theta_3 = 0, \cos\theta_2 + \cos\theta_3 = 0, \tag{33}$$

or

$$\cos\theta_2 - \cos\theta_3 = 0, \sin\theta_2 - \sin\theta_3 = 0. \tag{34}$$

Thus, Eqs. (33) and (34) yield Eqs. (31) and (32) to

$$\begin{aligned}&(\cos\beta_0 \sin\alpha_0 - \cos\alpha_0 \sin\beta_0 \cos\theta_1) \sin\theta_2\\ &\quad + \sin\beta_0 \sin\theta_1 \cos\theta_2 = 0,\end{aligned} \tag{35}$$

or

$$\begin{aligned}&(\cos\beta_0 \sin\alpha_0 - \cos\alpha_0 \sin\beta_0 \cos\theta_1) \cos\theta_2\\ &\quad + \sin\beta_0 \sin\theta_1 \sin\theta_2 = 0.\end{aligned} \tag{36}$$

Meanwhile, simplified element (3, 4) is

$$\begin{aligned}&\cos\theta_2 \sin\theta_1 + \cos\alpha_0 \cos^2\beta_0 - \cos^2\beta_0 \cos\theta_2 \sin\theta_1\\ &\quad - \cos\alpha_0 - \cos\alpha_0 \cos\theta_1 \sin\theta_2 + \cos\alpha_0 \cos\beta_0 \cos\theta_1 \sin\theta_2\\ &\quad + \cos\beta_0 \sin\alpha_0 \sin\beta_0(\cos\theta_1 + \sin\theta_2) = 0.\end{aligned} \tag{37}$$

This case is excluded because the curves of Eqs. (35) and (37), as well as Eqs. (36) and (37) intersect at several points, which means it is only satisfied in specific instantaneous configurations.

In summary, there are two sets of closure equations, i.e., $\theta_1 = \theta_4$, $\theta_2 = -\theta_3 = \theta_5 = -\theta_6$ and Eq. (29); $\theta_1 = \theta_4$, $\theta_2 = -\theta_3 = \pi - \theta_5 = \theta_6 + \pi$ and Eq. (30). When θ_2 was taken as the input of the kinematic variable, the other five variables are well determined, which means the *parallel 6-crease* kirigami pattern is rigidly foldable with one DOF. Additionally, the derived linkage is a type of parallel 6*R* linkage [27] with the parallel axes of three pairs of *R* joints, z_1 and z_4, z_2 and z_3 as well as z_5 and z_6.

The kinematic paths and corresponding configurations of this parallel 6*R* linkage are plotted in Fig. 10, where the geometric parameters with $\alpha_0 = 30°$, $\beta_0 = 45°$ are taken as an example. Two kinematic paths corresponding to Eqs. (29) and (30) intersect at points M $(\pi/2, \pi)$, M′ $(\pi/2, -\pi)$ and N $(-\pi/2, 0)$, indicating flat configurations ii and iv are bifurcation points (Fig. 10a). The linkage would move along path I if the corresponding pattern coupled with M-V assignments of configurations i and iii (M_I), whereas it would move along path II if the corresponding pattern coupled with M-V assignments of configurations v and vi (M_{II}). Meanwhile, kinematic variables θ_3, θ_5 and θ_6 versus θ_2 for paths I and II are illustrated in Fig. 10b and c, respectively.

The kinematic variables θ_i can be replaced by dihedral angles φ_i. For the *parallel 6-crease* kirigami pattern, the relationship between the kinematic variable θ_i and the dihedral angle φ_i is presented in Fig. 11a and b, which can be written as

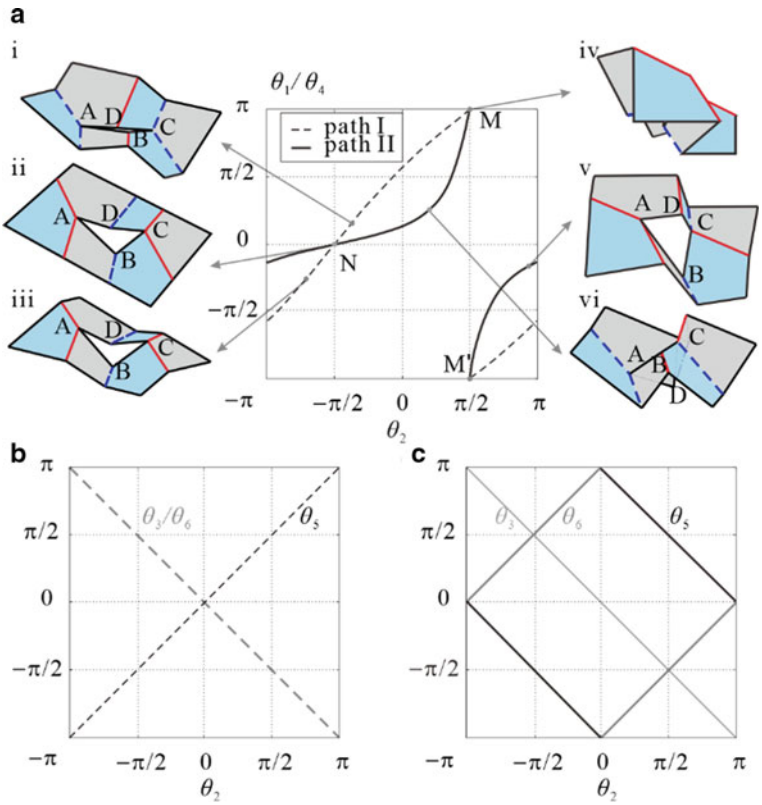

Fig. 10 Kinematic paths and corresponding configurations of the parallel 6*R* linkage with $\alpha_0 = 30°$, $\beta_0 = 45°$

$$\begin{aligned} &\theta_1 = \pi + \varphi_1, \quad \theta_2 = \pi/2 + \varphi_2, \quad \theta_3 = 3\pi/2 - \varphi_3, \\ &\theta_4 = \pi + \varphi_4, \quad \theta_5 = \pi/2 + \varphi_5, \quad \theta_6 = 3\pi/2 - \varphi_6, \end{aligned} \tag{38}$$

for kinematic path I, and

$$\begin{aligned} &\theta_1 = \pi + \varphi_1, \quad \theta_2 = \pi/2 + \varphi_2, \quad \theta_3 = 3\pi/2 - \varphi_3, \\ &\theta_4 = \pi + \varphi_4, \quad \theta_5 = \pi/2 - \varphi_5, \quad \theta_6 = \varphi_6 - \pi/2, \end{aligned} \tag{39}$$

for kinematic path II.

Thus, for both kinematic paths I and II, we have.

$$\varphi_1 = \varphi_4, \quad \varphi_2 = \varphi_3 = \varphi_5 = \varphi_6 \tag{40}$$

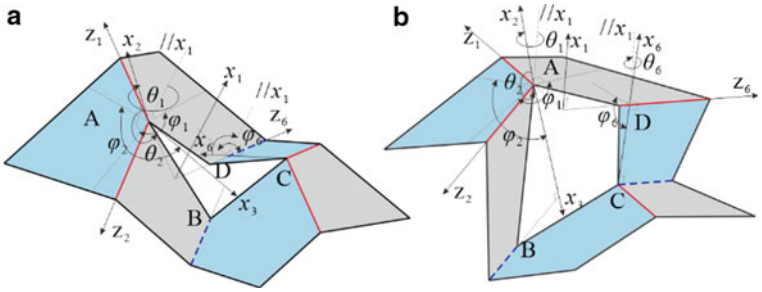

Fig. 11 The relationship between the kinematic variable and the dihedral angle for kinematic paths I and II

4 Tessellation of *Parallel 6-Crease* Kirigami Pattern

The possibility of building the tessellation of this *parallel 6-crease* kirigami pattern is also investigated. As shown in Fig. 12a, we join two mirrored copies of that unit along their shared boundaries E(E′)F(F′) in the horizontal direction. The new 4-crease vertices are formed at the intersection of panels, i.e., vertex G(G′) form by panels p_5, p'_5, p_6, p'_6 and vertex H(H′) form by panels p_5, p'_5, p_4, p'_4. The M-V assignments of creases DG, D′G′, CH, C′H′ are determined by the original kirigami pattern. The M-V assignments of crease EG and HF are the same as crease DG, and that of crease GH is the same as crease CH in the case of $\angle DGH < \pi/2$, and vice versa. According to the kinematic analysis of parallel 6*R* linkage, the dihedral angles of kirigami pattern always satisfy $\varphi_2 = \varphi_3 = \varphi_5 = \varphi_6$.

Since each basic unit has two types of M-V assignments, it is found that there are three rigidly foldable combinations for two mirrored units i.e., $M_I + M_I$, $M_{II} + M_{II}$ and $M_I + M_{II}$ (Fig. 12b). Hence, units are allowed to be connected compatibly with its mirror in the horizontal direction, as long as its M-V assignment satisfies the condition of rigid foldability in Fig. 10. Similarly, the units are compatible with its mirror image along the boundary I(I′)J(J′), which means the number of addable *parallel 6-crease* kirigami patterns is unlimited.

When the pattern is periodic in the vertical direction with the overlap of two neighboring units along crease A(A′)K(K′) and C(C′)L(L′), the tessellations of *parallel 6-crease* kirigami pattern are formed as shown in Fig. 13. It is noted that the tessellated structures in Fig. 13 are all 6 × 6 unit cells with three different M-V assignments. Specifically, the M-V assignment of the units in Fig. 13a has an alternating arrangement of M_I and M_{II} in the horizontal direction, while that of the units in Fig. 13b and c is a single type M_I or M_{II}, leading to approximating planar shape, arch shapes with different curvatures respectively. It is remarkable that they can switch to each other by changing the M-V assignment in a flat configuration due to the bifurcation of the kirigami unit. Furthermore, the construction method of combining *parallel 6-crease* kirigami patterns with different M-V assignments can also further form more complex structures, such as "m" shape (Fig. 14a) and closed-loop tube (Fig. 14b).

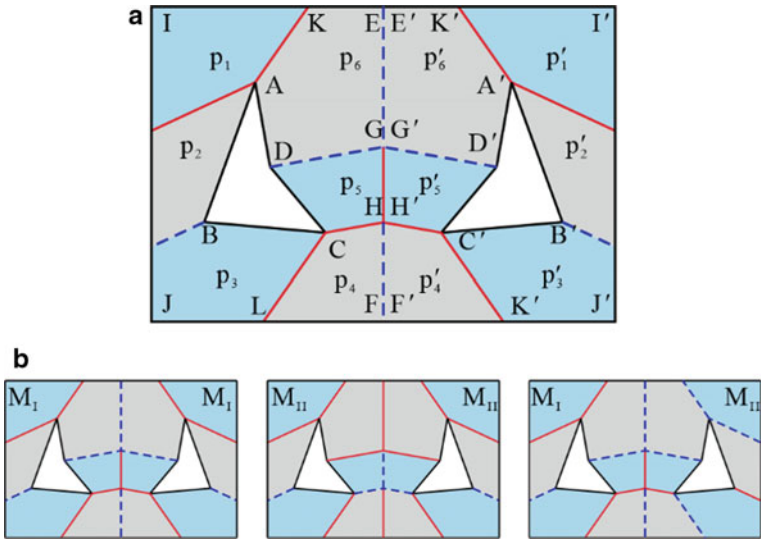

Fig. 12 Two *parallel 6-crease* kirigami patterns linked by 4-creases vertices

Note that all the kirigami units move synchronously and the one-DOF remains when units are combined.

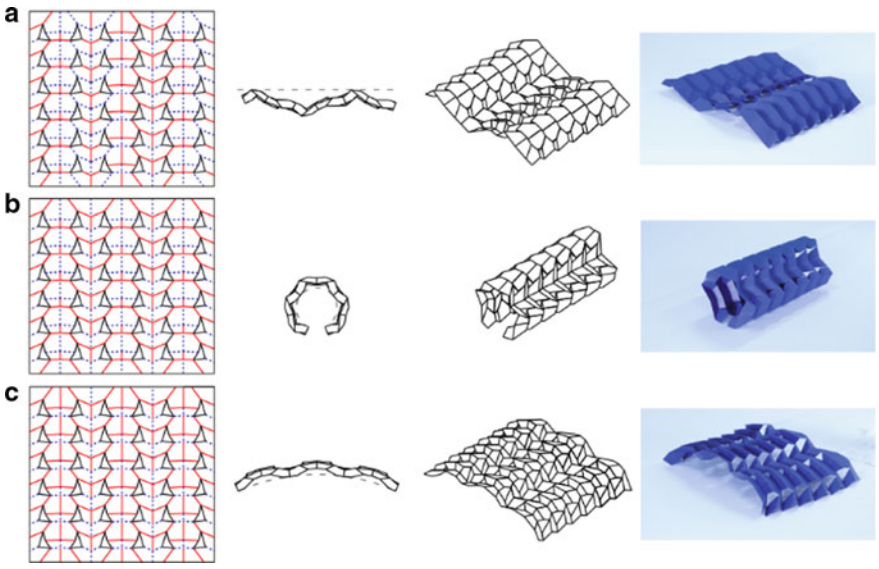

Fig. 13 Tessellations of *parallel 6-crease* kirigami pattern with 6 × 6 unit cells, where **a** is approximating planar shape, **b** and **c** are arch shapes with different curvatures

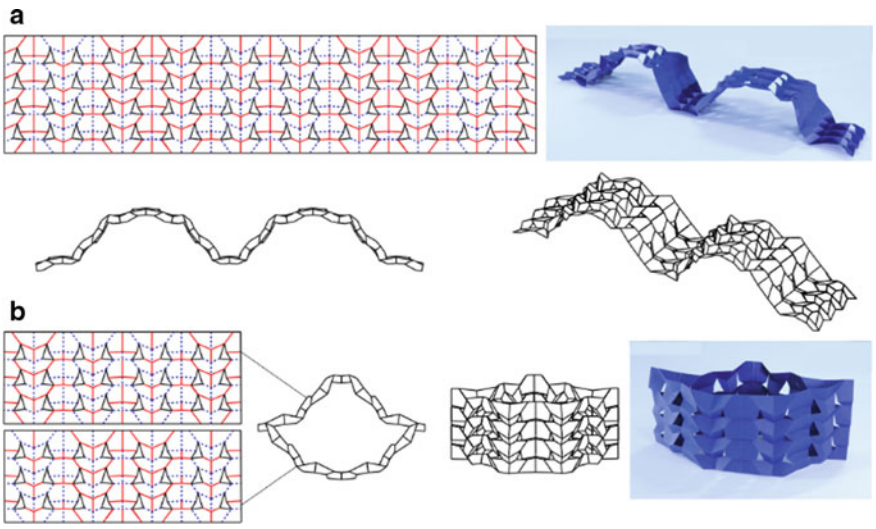

Fig. 14 Tessellations of *parallel 6-crease* kirigami pattern with **a** "m" shape and **b** closed-loop tube

5 Conclusions

This paper developed double-triangle mesh origami with flat foldability formed by four 4-crease vertices, whose rigid foldability and reconfigurability are discussed based on the motion compatibility of a multi-loop network with four spherical 4*R* linkages. We demonstrate that double-triangle mesh origami can be utilized as a platform for constructing reconfigurable 6*R* linkages through case studies on the evaluation of rigid foldability of a combination of two triangle twists. It can be seen that the kirigami patterns obtained from rigid origami (cases I and III) are always rigid, and the non-rigid origami pattern may result in a non-rigid kirigami pattern (case II), or it may be rigid (case IV). Hence, the rigid foldability of the origami pattern is a sufficient and unnecessary condition for the rigid foldability of the corresponding kirigami pattern. The reconfigurable 6*R* linkage can be constructed by first finding the geometric parameters that satisfy multiple sets of solutions, and then applying the kirigami technique to the double-triangle mesh origami. Three types of reconfigurable 6*R* linkage with one DOF have been derived from rigid kirigami patterns, including a double spherical linkage, a planar-spherical linkage, and a parallel 6*R* linkage. The motion sequences of the prototypes of the obtained patterns are shown in Table 1. A thorough kinematic study of the parallel 6*R* linkage has been conducted. Its bifurcation behavior is revealed by the matrix method, which provides valuable guidance for the tessellating *parallel 6-crease* kirigami pattern. Such reconfigurability further enhances its design flexibility to form larger homogeneous or heterogeneous structures with complex shapes. Although we have only discussed the tessellations of parallel 6-crease kirigami pattern, the construction method, i.e., combining configurations on different bifurcation paths, can be extended to other two rigid kirigami

patterns. An example of tessellation of the kirigami pattern of case III is shown in Appendix 3.

Table 1 The motion sequences of prototypes with $\alpha_0 = 30°$, $\beta_0 = 45°$

Variant cases	Unfolded state	Partly-folded state	Folded state	Rigid-foldable and reconfigurable
Origami pattern of case I		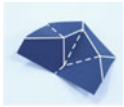		Yes
Kirigami pattern of case I	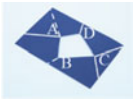			Yes
Origami pattern of case II		–	–	No
Kirigami pattern of case II	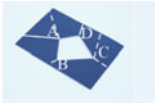	–	–	No
Origami pattern of case III				Yes
Kirigami pattern of case III				Yes
Origami pattern of case IV		–	–	No
Kirigami pattern of case IV				Yes

The geometric conditions of the patterns in case I and case III can be regarded as two sets of special solutions for compatible motions. However, due to the complexity of both the kinematic and geometric compatibility conditions, finding more sets of solutions remains a challenging and open question for our future study.

Acknowledgements Supported by National Natural Science Foundation of China (Grant Nos. 51825503, 52035008 and 51721003).

Appendix 1: D-H Notations

The Denavit-Hartenberg (D-H) coordinates are set up with geometric parameters and kinematic variables as illustrated in Fig. 15, where the axis z_i is along the revolute joint, x_i is the common normal from $z_{i\text{-}1}$ to z_i, and y_i follows right-hand rule. $a_{i(i+1)}$ is the length of link, i.e., the shortest distance between axes z_i and z_{i+1} along x_{i+1}. α_{i+1} is the twist angle from z_i to z_{i+1} positively about x_{i+1}. R_i is the offset from x_i to x_{i+1} positively about z_i. θ_i is the revolute variable of the linkage, which is the angle from x_i to x_{i+1} positively about z_i (Fig. 15).

For a single close-loop linkage consisted of n links, its closure equation is

$$T_{21}T_{32}\cdots T_{1n} = I, \tag{41}$$

where $\boldsymbol{I}$ is $n \times n$ identity matrix,

$$T_{(i+1)i} = \begin{bmatrix} \cos\theta_i & -\cos\alpha_{i(i+1)}\sin\theta_i & \sin\alpha_{i(i+1)}\sin\theta_i & a_{i(i+1)}\cos\theta_i \\ \sin\theta_i & \cos\alpha_{i(i+1)}\cos\theta_i & -\sin\alpha_{i(i+1)}\cos\theta_i & a_{i(i+1)}\sin\theta_i \\ 0 & \sin\alpha_{i(i+1)} & \cos\alpha_{i(i+1)} & R_i \\ 0 & 0 & 0 & 1 \end{bmatrix} \tag{42}$$

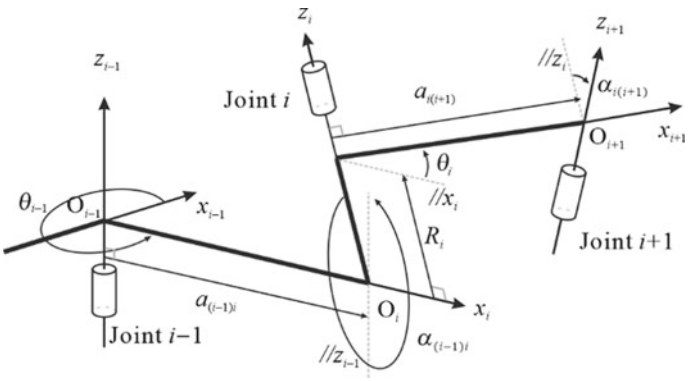

Fig. 15 Setup of the coordinate system and linkage geometric parameters

Appendix 2: Truss Method [28] on Kirigami Pattern of Case II

The equilibrium equation for a truss consisting of b bars and j joints can be written as

$$At = f, \tag{43}$$

where $\boldsymbol{A}$ is the $3j \times b$ equilibrium matrix, $\boldsymbol{t}$ is a $b \times 1$ vector of bar axial forces, and $\boldsymbol{f}$ is a $3j \times 1$ vector of node forces. If there are no external forces, then $\boldsymbol{f} = 0$. Equation (43) can be written as

$$At = 0. \tag{44}$$

The number of self-stresses s is

$$s = b - r, \tag{45}$$

where r is the rank of equilibrium matrix $\boldsymbol{A}$, and the number of mobility m is

$$m = 3j - 6 - r. \tag{46}$$

The parameters and M-V assignments of kirigami pattern of case II is shown in Fig. 16. For the truss form of the kirigami pattern of case, it contains $j = 14$ nodes and $b = 36$ bars. The coordinate of nodes can be as expressed as Eq. (47), when the geometric parameters are $\alpha_0 = 30°$, $\beta_0 = 45°$. The rank of the established equilibrium matrix is $r = 36$. Hence, the numbers of self-stresses and mobility of the pattern are $s = 0$, $m = 0$, and the kirigami pattern of case II is non-rigidly foldable.

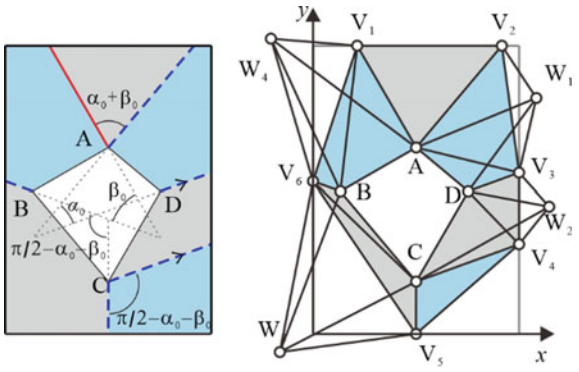

Fig. 16 Kirigami pattern of case ii and its truss form

$$
\begin{aligned}
V_1 &= \left[\,10.92623974\ 67\ 0\,\right]^T,\\
V_2 &= \left[\,43\ 67\ 0\,\right]^T,\\
V_3 &= \left[\,46\ 37.28216330\ 0\,\right]^T,\\
V_4 &= \left[\,46\ 20.13205456\ 0\,\right]^T,\\
V_5 &= \left[\,23.99962420\ 0\ 0\,\right]^T,\\
V_6 &= \left[\,0\ 35.94127398\ 0\,\right]^T,\\
A &= \left[\,23.99962420\ 44.35623388\ 0\,\right]^T,\\
B &= \left[\,36.53551505\ 33.83737249\ 0\,\right]^T,\\
C &= \left[\,23.99962420\ 12.12457262\ 0\,\right]^T,\\
D &= \left[\,5.78042184\ 33.83737249\ 0\,\right]^T,\\
M_1 &= \left[\,48.34508606\ 52.14108165\ 3.94329695\,\right]^T,\\
M_2 &= \left[\,50.77478333\ 28.28313885\ 2.41817698\,\right]^T,\\
M_3 &= \left[\,-8.93263306\ -13.59628895\ 16.30706331\,\right]^T,\\
M_4 &= \left[\,-9.93924684\ 67.96646390\ 9.84620205\,\right]^T.
\end{aligned}
\tag{47}
$$

Appendix 3: Tessellation of Kirigami Pattern of Case III

See Fig. 17.

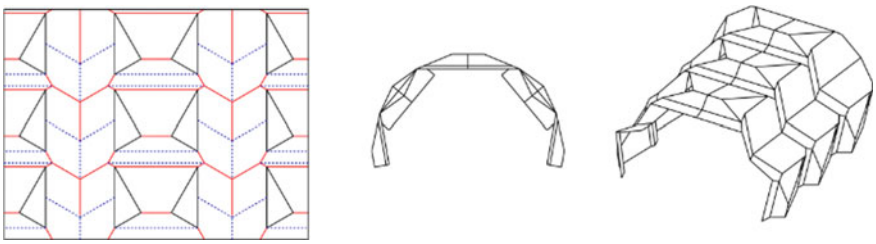

Fig. 17 Tessellations of kirigami pattern of case III

References

1. Lang RJ (2017) Twists, tilings, and tessellations: mathematical methods for geometric origami. CRC Press, Boca Raton, FL
2. Choi GP, Dudte LH, Mahadevan L (2019) Programming shape using kirigami tessellations. Nat Mater 18(9):999–1004
3. Boyvat M, Koh J-S, Wood RJ (2017) Addressable wireless actuation for multijoint folding robots and devices. Sci Robot 2(8):eaan1544
4. Zirbel SA, Lang RJ, Thomson MW, Sigel DA, Walkemeyer PE, Trease BP, Magleby SP, Howell LL (2013) Accommodating thickness in origami-based deployable arrays. J Mech Des 135(11):111005
5. Kuribayashi K, Tsuchiya K, You Z, Tomus D, Umemoto M, Ito T, Sasaki M (2006) Self-deployable origami stent grafts as a biomedical application of Ni-rich TiNi shape memory alloy foil. Mater Sci Eng A 419(1–2):131–137
6. Chen Y (2020) Review on Kinematic Metamaterials. J Mech Eng 56(19):2–13
7. Miura K (1985) Method of packaging and deployment of large membranes in space. Inst Space Astronaut Sci Rep 618:1–9
8. Evans TA, Lang RJ, Magleby SP, Howell LL (2015) Rigidly foldable origami twists. Origami, pp 119–130
9. Tachi T (2009) Generalization of rigid-foldable quadrilateral-mesh origami. J Int Assoc Shell Spat Struct 50(3):173–179
10. Peng R, Ma J, Chen Y (2018) The effect of mountain-valley folds on the rigid foldability of double corrugated pattern. Mech Mach Theory 128:461–474
11. Pratapa PP, Liu K, Paulino GH (2019) Geometric mechanics of origami patterns exhibiting Poisson's ratio switch by breaking mountain and valley assignment. Phys Rev Lett 122(15):155501
12. Pratapa PP, Liu K, Vasudevan SP, Paulino GH (2021) Reprogrammable kinematic branches in tessellated origami structures. J Mech Robot 13(3):031004
13. Dai JS, Rees Jones J (1999) Mobility in metamorphic mechanisms of foldable/erectable kinds. J Mech Des 121(3):375–382
14. Chen Y, Lv W, Peng R, Wei G (2019) Mobile assemblies of four-spherical-4R-integrated linkages and the associated four-crease-integrated rigid origami patterns. Mech Mach Theory 142:103613
15. Liu S, Chen Y, Lu G (2013) The rigid origami patterns for flat surface. In: Proceedings of the international design engineering technical conferences and computers and information in engineering conference, American Society of Mechanical Engineers, p V06BT07A039
16. Wang K, Chen Y (2011) Folding a patterned cylinder by rigid origami. Origami, pp 265–276
17. Zhang K, Dai JS (2016) Reconfiguration of the plane-symmetric double-spherical 6R linkage with bifurcation and trifurcation. Proc Inst Mech Eng C J Mech Eng Sci 230(3):473–482
18. Zhang K, Dai JS (2016) Geometric constraints and motion branch variations for reconfiguration of single-loop linkages with mobility one. Mech Mach Theory 106:16–29
19. Wei G, Dai JS (2014) Origami-inspired integrated planar-spherical overconstrained mechanisms. J Mech Des 136(5):051003
20. Ma X, Zhang K, Dai JS (2018) Novel spherical-planar and Bennett-spherical 6R metamorphic linkages with reconfigurable motion branches. Mech Mach Theory 128:628–647
21. Feng H, Peng R, Ma J, Chen Y (2018) Rigid foldability of generalized triangle twist origami pattern and its derived 6R linkages. J Mech Robot 10(5):051003
22. Liu W, Chen Y (2020) A double spherical 6R linkage with spatial crank-rocker characteristics inspired by kirigami. Mech Mach Theory 153:103995
23. Wang R, Song Y, Dai JS (2021) Reconfigurability of the origami-inspired integrated 8R kinematotropic metamorphic mechanism and its evolved 6R and 4R mechanisms. Mech Mach Theory 161:104245
24. Hartenberg RS, Denavit J (1955) A kinematic notation for lower pair mechanisms based on matrices. J Appl Mech 77(2):215–221

25. Evans TA, Lang RJ, Magleby SP, Howell LL (2015) Rigidly foldable origami gadgets and tessellations. Roy Soc Open Sci 2(9):150067
26. Goldberg M (1943) New five-bar and six-bar linkages in three dimensions. Trans ASME 65:649–661
27. Li Z, Schicho J (2014) Three types of parallel 6R linkages. Computational kinematics. Springer, pp 111–119
28. Yang F, Chen Y, Kang R, Ma J (2016) Truss transformation method to obtain the non-overconstrained forms of 3D overconstrained linkages. Mech Mach Theory 102:149–166